The American Journal of Pathology, Vol. 184, No. 6, June 2014

The American Journal of
PATHOLOGY
ajp.amjpathol.org

TUMORIGENESIS AND NEOPLASTIC PROGRESSION

Recruitment of CD34$^+$ Fibroblasts in Tumor-Associated Reactive Stroma

The Reactive Microvasculature Hypothesis

Rebeca San Martin,* David A. Barron,* Jennifer A. Tuxhorn,* Steven J. Ressler,* Simon W. Hayward,† Xiaoyun Shen,‡ Rodolfo Laucirica,‡ Thomas M. Wheeler,‡ Carolina Gutierrez,‡ Gustavo E. Ayala,‡ Michael Ittmann,§ and David R. Rowley*

From the Departments of Molecular and Cellular Biology, and Pathology and Immunology,‡ Baylor College of Medicine, Houston, Texas; the Department of Urology,† Vanderbilt University, School of Medicine, Nashville, Tennessee; and the Department of Pathology and Laboratory Medicine, Michael E. DeBakey VA Medical Center,§ Houston, Texas*

Accepted for publication February 19, 2014.

Address correspondence to David R. Rowley, Ph.D., Department of Molecular and Cellular Biology, Baylor College of Medicine, One Baylor Plaza, 514B, mail stop BCM130, Houston, TX 77030. E-mail: drowley@bcm.edu.

Reactive stroma co-evolves with cancer, exhibiting tumor-promoting properties. It is also evident at sites of wound repair and fibrosis, playing a key role in tissue homeostasis. The specific cell types of origin and the spatial/temporal patterns of reactive stroma initiation are poorly understood. In this study, we evaluated human tumor tissue arrays by using multiple labeled, quantitative, spectral deconvolution microscopy. We report here a novel CD34/vimentin dual-positive reactive fibroblast that is observed in the cancer microenvironment of human breast, colon, lung, pancreas, thyroid, prostate, and astrocytoma. Recruitment of these cells occurred in xenograft tumors and Matrigel plugs *in vivo* and was also observed in stromal nodules associated with human benign prostatic hyperplasia. Because spatial and temporal data suggested the microvasculature as a common site of origin for these cells, we analyzed microvasculature fragments in organ culture. Interestingly, fibroblasts with identical phenotypic properties and markers expanded radially from microvasculature explants. We propose the concept of reactive microvasculature for the evolution of reactive stroma at sites of epithelial disruption common in both benign and malignant disorders. Data suggest that the reactive stroma response is conserved among tissues, in normal repair, and in different human cancers. A more clear understanding of the nature and origin of reactive stroma is needed to identify novel therapeutic targets in cancer and fibrosis. *(Am J Pathol 2014, 184: 1860–1870; http://dx.doi.org/10.1016/j.ajpath.2014.02.021)*

Recruitment and accumulation of reactive stroma cells occurs relatively early during the initiation of carcinoma *in situ* and exhibits a focal pattern associated with some, but not all, early carcinomas. We have reported previously that reactive stroma initiates early during prostate cancer tumorigenesis, with foci being observed during premalignant prostatic intraepithelial neoplasia (PIN).[1,2] Reactive stroma is characterized by the presence of vimentin (VIM)$^+$ stromal cells that have been termed carcinoma-associated fibroblasts (CAFs), and myofibroblasts that are positive for smooth muscle alpha actin (ACTA2) and VIM. This response is not exclusive to cancer and occurs during normal wound repair and at sites of epithelial damage.[3,4] Accordingly, it has been proposed that tumor-associated reactive stroma essentially serves a wound repair function at sites of disrupted tissue homeostasis.[5] CAFs function to foster tumor growth in the breast,[6,7] prostate,[8,9] and pancreas.[10] Both myofibroblasts and CAFs remodel the extracellular matrix directly via deposition of collagen type I,[11–13] tenascin C,[2,9,14] and expression of matrix metalloproteinases.[15,16] The tumor microenvironment biology affected by

Supported by NIH grants U54 CA126568, R01 CA58093, and R01 DK083293 (D.R.R.); National Cancer Institute Cancer Center Support grant P30 CA125123; and NIH Breast Cancer SPORE grant P50 CA58183.

Disclosures: None declared.

Current address of D.A.B., Department of Radiation Oncology, Memorial Sloan-Kettering Cancer Center, New York, NY; of J.A.T., Wyle Science, Technology, and Engineering Group, Houston, TX; of S.J.R., Aptalis Pharma, Bridgewater, NJ; of X.S., Department of Pediatrics, Texas Children's Hospital, Houston, TX; of G.E.A, Department of Pathology, University of Texas Medical School, Houston, TX.

http://dx.doi.org/10.1016/j.ajpath.2014.02.021

CAFs and myofibroblasts likely fosters the progression of cancer via differential adhesion patterns and transient epithelial-to-mesenchymal transition induction[17–20] in addition to modulating rates of angiogenesis.

Little is understood about initiation of reactive stroma, the specific cell types of origin, and the biology that regulates its activation and recruitment. Moreover, the relationship between CAFs and myofibroblasts and whether these phenotypes represent different cells or different states of a common cell are not understood. In addition, it is not known whether different human tumors share a common pattern of recruitment and composition of stromal cell types in their respective microenvironments. These questions are important because novel therapeutics designed strategically to target common microenvironment biology may be effective treatments for several different cancers and other proliferative disorders.

To address these issues, the National Cancer Institute funded Tumor Microenvironment Network program initiated a study to evaluate human tissue arrays derived from patients with prostate, breast, colon, pancreas, lung, thyroid, and brain cancer for common tumor microenvironment markers. We report here that a novel population of CD34/VIM dual-positive fibroblasts was consistently identified within the tumor microenvironment of several different human cancers. Moreover, similar recruitment patterns were observed in human benign prostatic hyperplasia (BPH), in mouse models of reactive stroma, and in the initial reactive stroma recruited to human xenograft tumors. Additional experiments with isolated microvasculature indicated a vessel wall origin. Accordingly, we propose here a common reactive microvasculature hypothesis for the initiation and co-evolution of reactive stroma fibroblasts commonly observed in cancers, benign disorders, and wound repair.

Materials and Methods

Tissue Arrays

All tissue arrays were generated and evaluated under approval by institutional review boards and provided by Baylor College of Medicine (prostate, mammary, lung), Vanderbilt University (colon), or purchased commercially (pancreas, thyroid, and brain) as follows. Prostate tissue array was provided by Gustavo Ayala and Tom Wheeler, Dan L. Duncan Cancer Center, Baylor College of Medicine (Houston, TX). The six-slide set contained samples from 50 cases of adenocarcinoma, confirmed by histopathology, with adjacent PIN and normal tissues from the same patients. In total, 97 normal, 94 PIN, and 92 cancer cores provided usable information for quantitation. The cancer cores exhibited a Gleason sum score of 5 (5 cores), Gleason 6 (59 cores), and Gleason 7 (30 cores), representing a range and frequency typical of most radical prostatectomy samples. Breast tissue array was provided by Kent Osborne, Breast Center, Dan L. Duncan Cancer Center, Baylor College of Medicine. One unique slide contained 4 normal and 48 cancer tissue samples. Colon tissue array was provided by Robert Coffey and Simon Hayward, Vanderbilt Ingram Center, Vanderbilt University Medical Center (Nashville, TN). One unique slide contained 22 normal and 110 cancer tissue samples. Pancreas tissue array was purchased from Biochain (catalog no. Z7020090; Hayward, CA). One slide contained 3 normal and 45 cancer tissue samples. Lung tissue array was constructed and provided by Xioyun Shen, Rodolfo Laucirica, and Tom Wheeler, Department of Pathology, Baylor College of Medicine. One unique slide contained 61 cases of adenocarcinoma, confirmed by diagnosis, and adjacent paired matched normal tissue. Brain tissue array was purchased from Biochain (catalog no. Z5070004). One slide contained 4 normal and 59 cancer tissue samples. Thyroid tissue array was purchased from Biochain (catalog no. Z7020098). One slide contained 3 normal and 93 cancer tissue samples (including inflammatory diseases). Archival BPH tissue was obtained from patients undergoing surgical treatment and provided by the Department of Pathology, Baylor College of Medicine, and handled as described previously.[21]

Animals

Athymic NCr-*nu/nu* male homozygous nude mice, between 6 and 8 weeks of age, were obtained from Charles River Laboratories (Wilmington, MA). *Flk1-myr::mCherry*$^{+/tg}$ mice were a kind gift from Dr. Mary Dickinson at Baylor College of Medicine. Transgenic mice expressing active transforming growth factor (TGF)-β1 targeted to prostate epithelial cells were generated as reported previously.[22] Mice housing and manipulations followed approved protocols from the Institutional Animal Care and Use Committee.

Cell Lines

LNCaP human prostate carcinoma cells (ATCC, Manassas, VA) were cultured in RPMI 1640 (Life Technologies, Inc., Rockville, MD), which was supplemented with 10% fetal bovine serum (Hyclone, Logan, UT), 100 U/mL penicillin, and 100 μg/mL streptomycin (Sigma Chemical Co., St. Louis, MO).

Preparation of Xenograft Tumors

Xenograft tumors were generated in NCr-*nu/nu* mice under two-way (Matrigel and LNCaP cells) conditions as previously described.[23–26] Briefly, 16×10^6 LNCaP cells were resuspended in 300 μL of complete medium, incubated on ice, and mixed with 500 μL of thawed Engelbreth-Holm-Swarm Matrigel extracellular matrix (Becton Dickinson, Bedford, MA). Mice were injected subcutaneously in both lateral flanks with 100 μL of the LNCaP cell-Matrigel mix (2×10^6 cells), using a total of three animals per experiment (six tumors). For control Matrigel plugs, 100 μL of Matrigel without cells was injected per site in a similar manner.

Xenografts were harvested at different time points, between 4 and 21 days, dissected from skin, and fixed in 4%

paraformaldehyde overnight at 4°C. Tissues were then washed three times with PBS, processed for histology by embedding in paraffin, and cut into sections at a nominal thickness of 5 μm. After histological evaluation with H&E, the following time points were used for further immunohistochemistry (IHC) experiments: day 4, day 10, and day 12 for Matrigel plugs and day 10 and day 21 for LNCaP-Matrigel xenografts.

IHC

Tissue Arrays

All tissue arrays were evaluated with multiple-label IHC and spectral deconvolution microscopy. Primary antibodies for CD34 (MS-363-P 1:100; Thermo Scientific, Waltham, MA), and VIM (MS-129-P 1:50; Thermo Scientific) were evaluated for specificity, and staining conditions were optimized empirically. IHC was conducted with a multiplex staining kit according to the manufacturer's instructions (Biocare Medical, Concord, CA). Briefly, tissues were subjected to heat-induced antigen retrieval, using citrate buffer, pH 6, for 25 minutes. Sections were incubated with the VIM primary antibody for 30 minutes at room temperature, followed by application of Mach3 probe (Biocare Medical) and Mach poly alkaline phosphatase (AP; Biocare Medical), each for 15 minutes at room temperature. Fast Red chromogen (Biocare Medical) was added and developed for 10 minutes at room temperature, according to the manufacturer's instructions. Biocare denaturing reagent was then added for 5 minutes to disrupt the antibody-polymer interaction. Tissues were then incubated in the CD34 primary antibody for 25 minutes at room temperature, followed by application of Mach3 probe (Biocare Medical) and Mach3 Poly horseradish peroxidase (HRP; Biocare Medical) each for 12 minutes. Slides were incubated in diaminobenzidine for another 5 minutes, dehydrated, and permanently mounted for analysis.

Xenograft Tumors and Matrix Traps

Immunostaining was performed with the MicroProbe Staining System (Fisher Biotech, Pittsburgh, PA), and capillary action optimized reagents from Open Biosystems (Huntsville, AL) as follows: paraffin-embedded, 5-μm sections were dewaxed by using xylene and were hydrated through a series of graded ethanol. Sections were then subjected to heat-induced antigen retrieval with the use of citrate buffer, pH 6, for 20 minutes. After cooling, endogenous peroxidase activity was blocked by treating with 3% H_2O_2 in PBS for 10 minutes at room temperature. Blocking was performed by subsequent incubation in Protein Blocker (GTX30963, Gentex, Irvine, CA) for 5 minutes at 50°C, followed by 5% goat serum for 30 minutes at room temperature. Samples were incubated overnight at 4°C with a mixture of the primary antibodies as follows: monoclonal rat anti-mouse for CD34 (ab8158 1:250; Abcam, Cambridge, MA) and monoclonal rabbit anti-mouse VIM (ab92547 1:100; Abcam), diluted in primary antibody diluent. For human BPH tissues, a mixture of monoclonal mouse anti-human CD34 (IR632 1:50; Dako, Carpinteria, CA) and monoclonal rabbit anti-human VIM (ab133260 1:250; Epitomics-Abcam, Burlingame, CA) was used.

Samples were exposed to a mixture of secondary antibodies for 45 minutes at 37°C as follows: biotinylated goat anti-rat, or mouse as needed (A10517 or A10676 1:500; Molecular Probes, Eugene, OR) diluted in ready-to- use HRP-conjugated, goat anti-rabbit (3051-1; Epitomics-Abcam). Color was developed by using a combination of AP-HPR substrates, according to the manufacturer's instructions (Vector Laboratories, Burlingame, CA). First, to detect CD34, sections were exposed to avidin-bound AP (Vectastain ABC kit, AK-5000; Vector Laboratories) for 30 minutes, followed by 15-minute incubation in its substrate (AP substrate Kit III, SK5300; Vector Laboratories). VIM was detected by incubating sections in HRP substrate ImmPACT Nova Red (SK4805; Vector Laboratories) for 10 minutes. Sections were counterstained with methyl green (H-3402; Vector Laboratories) for 3 minutes at 60°C, dehydrated through a series of graded ethanol, and washed for 5 minutes in Histoclear (HS-200; National Diagnostics, Atlanta, GA). All samples were mounted in the non−Xylene-based media Vectamount (H-5000; Vector Laboratories).

Human BPH Samples

Special consideration was given to retrieval for archival BPH samples as follows: after deparaffinization, endogenous peroxidase activity was blocked by incubating the samples in 3% hydrogen peroxide/PBS. Slides were then washed in water and transferred into a Coplin jar filled with a 1% zinc sulfate solution. This jar was placed in a 500-mL beaker that contained 150 mL of 1% zinc sulfate solution. After sealing with vented plastic wrap, the assembly was microwaved for 5 minutes at 50% power, stopping half way to replenish the zinc sulfate solution in the inner chamber as needed. Slides were then allowed to cool down, inside the zinc sulfate solution, for 15 minutes at room temperature before being transferred to the microprobe slide holder for blocking and subsequent steps as listed in *Xenograft Tumors and Matrix Traps*.

Antibody Validation

Antibodies were validated for specificity and dynamic concentration range by using normal human prostate samples as control tissue and test slides from the prostate tissue array. The antibodies were titered on these samples, within the manufacturer's suggested range, to determine the optimal working concentration. In all cases, antibodies chosen showed consistent staining of relevant structures as positive controls (blood vessels), or compartments (stromal cells), with decreased color intensity at the dilute concentrations. Samples in which the primary antibody was omitted were used as negative control and to verify the absence of secondary antibody nonspecific binding. Consistent staining between normal tissue samples and the tissue microarray test slides confirmed that the antibodies produced reproducible results.

Multispectral Imaging

Multispectral imaging was performed with a Nikon Labophot-2 microscope, equipped with a Nikon PlanApo 40× objective (144756) coupled to a Nuance spectral deconvolution camera and software (model no. N-MSI-420F2) from PerkinElmer−Caliper Biosciences (Hopkinton, MA). The Nuance software platform version 3.0.0 was used for all image acquisition, spectral deconvolution, and colocalization analysis. With the use of the bright field capture mode and an empty visual field as reference, a cube of images was acquired by automatic stacking of images taken at 20-nm increments that spanned the camera's spectral range, from 420 to 720 nm. A clockwise, unbiased pattern of image acquisition was used, to ensure 100% coverage of each microarray sample at ×40 magnification. After construction of a spectral library for Fast red, Nova Red, diaminobenzidine, Vector blue, hematoxylin, and methyl green, image cubes were spectrally deconvoluted for the necessary channels and pseudo-colored for the biomarkers. Thresholding of each signal was determined as the pixel density average from all normal tissue-acquired cubes. After manually processing all normal sample cubes, frequency histograms of the percentage of positive area for all normal tissues were constructed. A reference cube whose pixel densities fell at −2 SD from the mean was chosen as the reference for batch colocalization analysis. For all tissue arrays, percentage of signal and colocalization, using either hematoxylin or methyl green counterstain as a denominator for total pixel count, was computationally determined with the Nuance software version 3.0.0 for each multispectral cube. For microvasculature culture, colocalization was determined as the percentage of pixels positive for blue (CD34) within pixels positive for red (VIM), because the samples were not counterstained.

Microvasculature Explant Culture

Microvasculature explants were obtained with the protocol by Reed,[27] with modifications. Briefly, the abdominal adipose tissue from three *Flk1-myr::mCherry*$^{+/tg}$ mice was collected, rinsed thoroughly with cold PBS, and chopped into small fragments with the use of sterile scissors, carefully removing lymph nodes, if present. All fat was pooled into 20 mL of a solution of 2 mg/mL bovine serum albumin (Invitrogen, Carlsbad, CA), 2 mg/mL Collagenase (catalog no. 17018-029; Gibco, Carlsbad, CA) in Dulbecco's modified Eagle's medium high glucose (catalog no. 11965167; Invitrogen) and allowed to digest for 40 minutes, at 37°C, with horizontal agitation (200 rpm). The resulting digest was centrifuged at 1000 × *g* for 5 minutes, and the supernatant was discarded. The pellet was resuspended in 8 mL of microvasculature (MV) media (Dulbecco's modified Eagle's medium high glucose that contained 10% fetal bovine serum, 100 U/mL penicillin, 100 μL/mL streptomycin) and was centrifuged again under the same conditions as before. The second pellet was resuspended again in 8 mL of MV media and filtered through a Nitex 300-μm membrane to eliminate tissue remnants. The filtrate was then filtered again through a Nitex 30-μm membrane, which retains the microvasculature fragments while allowing single cells to go through.

The membrane was inverted over a 60-mm cell culture dish and washed thoroughly with 2 mL of MV media to collect the microvasculature fragments. For low-density culture, done in six-well plates, 200 μL of this extract was seeded in coverslips that were previously coated with a thin layer of Matrigel (BD Biosciences, Billerica, MA), diluted to a concentration of 3 mg/mL. Five minutes after seeding, 2 mL of MV media was added to each well, and cultures were incubated at 37°C, 5% CO_2 for 24 and 48 hours. Explants were fixed by adding 2 mL of 8% paraformaldehyde pH 7.4, followed by 20 minutes of incubation at room temperature. Microvasculature explant culture coverslips were then washed with PBS, with gentle shaking, three times (5 minutes each), at room temperature to eliminate all paraformaldehyde and were stored in PBS at 4°C.

Immunocytochemistry

Microvasculature explant culture coverslips were washed with PBS, with gentle shaking, three times (5 minutes each), at room temperature. Cells were permeabilized by incubation in 0.1% Triton X-100 in PBS at room temperature for 5 minutes, followed by PBS washes as before. Coverslips were then incubated in 1% goat serum (Sigma Chemical Co.) in PBS for 30 minutes at room temperature to block unspecific binding. Primary antibodies were mixed together in primary antibody diluent (Open Biosystems) as follows: VIM rabbit anti-mouse monoclonal (ab92547 1:250; Abcam) and CD34 rat anti-mouse monoclonal (catalog no. 8158, 1:50; BioLegend, San Diego, CA). Samples were incubated in primary antibodies overnight, at 4°C. After washing, endogenous peroxidase activity was blocked by incubation in 0.3% hydrogen peroxide in methanol for 10 minutes, at room temperature, followed by a PBS wash.

Biotinylated goat anti-rat secondary antibody (A10517; Molecular Probes) was diluted at 1:500 in goat anti-rabbit HRP-conjugated secondary antibody (3051-1; Epitomics-Abcam). Samples were exposed to the secondary antibody mixture in a humidified chamber for 45 minutes at 37°C. Color development was performed as described in *IHC*, using AP-Vector Blue for CD34 detection and HRP-ImmPACT Nova Red (Vector Laboratories) for VIM. Finally, coverslips were washed in water and mounted, without dehydration, with the use of Fluormount (catalog no. F4680; Sigma Chemical Co.).

Statistical Analysis

Quantification data subsets per tissue were analyzed with Kruskal-Wallis nonparametric analysis of variance, and Dunn's posttest to compare paired sets to determine significant differences between groups ($P < 0.01$).

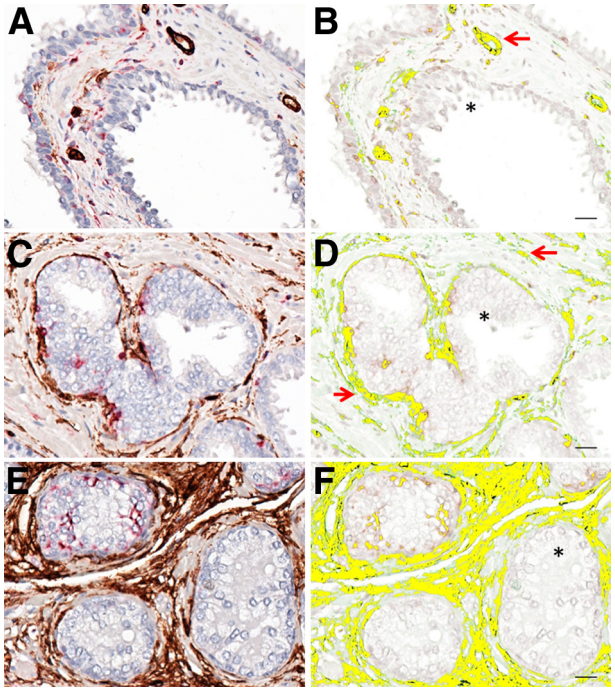

Figure 1 The prostate tissue arrays consisted of 32 normal cores that resulted in 420 multispectral cubes, 25 PIN cores that resulted in 333 multispectral cubes, and 27 cancer cores that resulted in 371 multispectral cubes. **A**, **C**, and **E:** Representative RGB micrographs show an increase in CD34/VIM staining that correlates with cancer progression. **B**, **D**, and **F:** CD34/VIM colocalization is pseudo-colored yellow and shows epithelial acini (**asterisks**), vasculature (**red arrows**). Shown are normal prostate (**A** and **B**), PIN (**C** and **D**), and cancer (**E** and **F**). Original magnification: ×400. Scale bars: 20 μm (**B**, **D**, and **F**). RGB, red, green, and blue.

Results

CD34/VIM Dual-Positive Cells Are Associated with the Reactive Stroma of Different Human Cancers

A total of 2200 multispectral cubes were obtained from the prostate microarray. Dual IHC deconvolution indicated that in normal prostate, most CD34/VIM dual-positive cells localized to the vascular walls of blood vessels adjacent to secretory epithelial acini (Figure 1, A and B). A vascular and perivascular pattern was also observed at focal sites of PIN. In contrast to normal tissues, an enrichment of single cells, sometimes observed in sheets or clusters that exhibit dual-positive immunoreactivity, was observed in the stroma adjacent to PIN foci (Figure 1, C and D) and in prostatic adenocarcinoma (Figure 1, E and F). The sheets of dual-positive cells were not immediately associated with the vessel wall as confirmed by platelet endothelial cell adhesion molecule 1 (PECAM1; CD31) staining (data not shown).

A total of 273 multispectral cubes were acquired from the human brain cancer microarray. In normal encephalon dual-positive cells were few and were primarily associated with vessel walls (Figure 2, A and B). In lower tumor grades, elevated numbers of CD34/VIM$^+$ cells were spatially associated in a radial pattern adjacent to vascular walls (Figure 2, C and D). Similar to prostate carcinoma, CD34/VIM$^+$ cells appear as clusters or sheets intermingled with astrocytoma cells. This was particularly evident in higher grade tumors that exhibited sheets of CD34/VIM dual-positive cells with a fibroblast-like morphology (Figure 2, E and F). In addition, an increase in heterogeneity of staining patterns was progressively associated with advanced disease stages, compared with normal.

Evaluation of the pancreatic cancer array (146 spectral cubes) showed similar patterns of distribution of CD34/VIM$^+$ cells with a fibroblast morphology associated with regions of carcinoma (Figure 3, C–F) relative to control (Figure 3, A and B).

A statistically significant enrichment of the CD34/VIM dual-positive population was observed in prostate cancer ($P < 0.001$) when the percentage of colocalization values were compared with normal (Figure 4A). Quantitation of data also showed that a significant enrichment of CD34/VIM dual-positive population was associated with increasing tumor grade in astrocytoma ($P < 0.001$) (Figure 4B). In the pancreas tissue array, an increase in heterogeneity of staining patterns and quantity was associated with more advanced grades of tumors (Figure 4C), but the marked heterogeneity of CD34/VIM dual-positive staining patterns in pancreatic cancer and the lack of

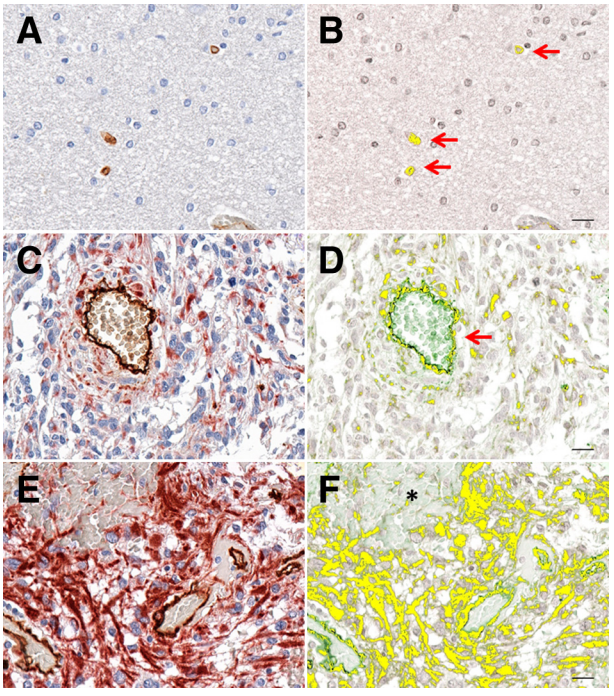

Figure 2 The brain tumor tissue array consisted of 63 tissue cores, resulting in 273 multispectral cubes. **A**, **C**, and **E:** Representative RGB micrographs show an increase in CD34/VIM staining that correlates with cancer progression. **B**, **D**, and **F:** CD34/VIM colocalization is pseudo-colored yellow and shows astrocytoma cell (**asterisk**), vasculature (**red arrows**). Shown are normal encephalon (**A** and **B**), astrocytoma grade I (**C** and **D**), and astrocytoma grade II (**E** and **F**). Original magnification: ×400 (**A**, **C**, and **E**). Scale bars: 20 μm (**B**, **D**, and **F**). RGB, red, green, and blue.

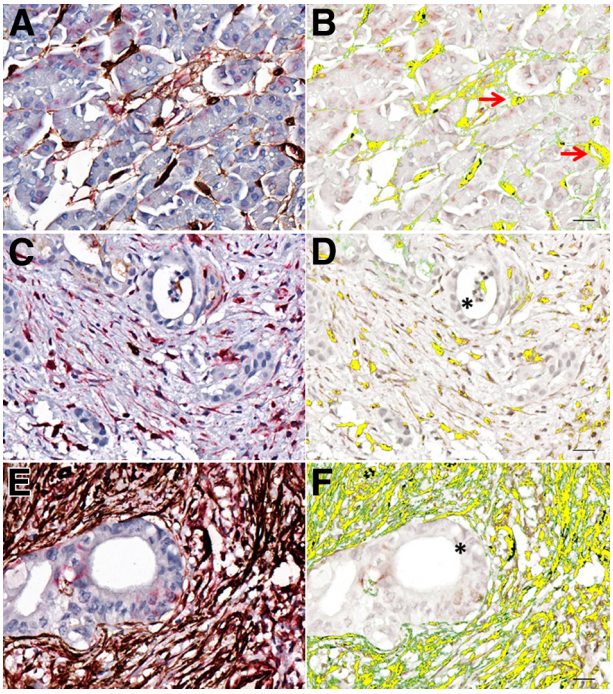

Figure 3 The pancreas tissue array consisted of 48 tissue cores, resulting in 146 multispectral cubes. **A**, **C**, and **E:** Representative RGB micrographs show an increase in CD34/VIM staining that correlates with cancer progression. **B**, **D**, and **F:** CD34/VIM colocalization is pseudo-colored yellow and shows adenocarcinoma foci (**asterisks**) and vasculature (**red arrows**). Shown are normal pancreas (**A** and **B**), adenocarcinoma grade I (**C** and **D**), and adenocarcinoma grade II (**E** and **F**). Original magnification: ×400 (**A**, **C**, and **E**). Scale bars: 20 μm (**B**, **D**, and **F**). RGB, red, green, and blue.

sufficient normal samples in this tissue array precluded statistical evaluation.

We also analyzed spectral cubes acquired from the colon cancer array (206 cubes) (Supplemental Figure S1), a breast cancer array (373 cubes) (Supplemental Figure S2), a lung cancer array (760 cubes) (Supplemental Figure S3), and a thyroid cancer array (Supplemental Figures S4 and S5). In colon cancer tissues, the spatial distribution and phenotype of CD34/VIM$^+$ stromal cells were nearly identical to other cancer tissues. A trend toward enrichment related to cancer grade was observed; however, it was not statistically significant (data not shown). In mammary cancer tissues, CD34/VIM$^+$ cells were also observed in regions associated with focal areas of carcinoma. Interestingly, a trend toward depletion of dual-positive cells was observed in intraductal carcinoma; however, the absence of a sufficient normal population in the tissue array precluded statistical analysis. Evaluation of lung cancer samples also showed CD34/VIM dual-positive cells with similar spatial patterns emerging in the tumor microenvironment. Interpretation in lung tissue was precluded by the large vessel density, low volume of stroma, and heterogeneity relative to other tissues. Spectral deconvolution of the 273 cubes acquired from the human thyroid microarray also showed enrichment in dual-positive cells that associate with all grades of thyroid cancer compared with normal samples. However, focal areas of thyroid cancer also exhibited some VIM and CD34 staining in carcinoma cells, precluding a meaningful statistical evaluation. This appeared to be carcinoma specific and was not observed, however, in thyroid tissues with inflammatory phenotypes such as Hashimoto's thyroiditis (Supplemental Figure S4) which were included in the tissue array.

CD34/VIM$^+$ Cells in Human BPH Periurethral Stromal Nodules

Human BPH tissue was examined to assess whether recruitment of CD34/VIM$^+$ stromal cells to reactive stroma was a common response in benign tissue remodeling in proliferative disorders. Interestingly, hyperplastic stromal nodules adjacent to the urethra were positive for CD34/VIM$^+$ cells (Figure 5, A and B) with a spatial distribution pattern and phenotype similar to those observed in carcinoma tissue. Notably, central regions in these nodules exhibited an elevated density of several closely situated blood vessels that appeared to be arterioles or small muscular arteries (Figure 5, B–D). The spatial pattern of CD34/VIM$^+$ fibroblast-appearing cells was in close

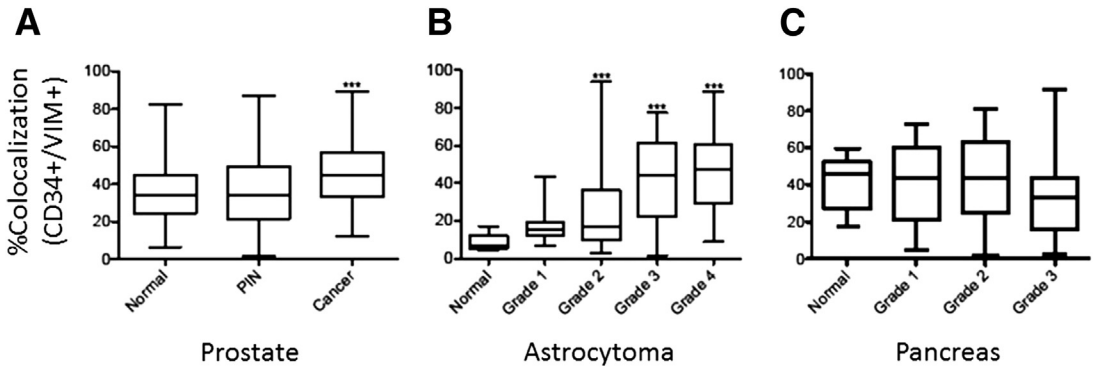

Figure 4 A statistically significant increase is present in the percentage of colocalization of CD34 and VIM in prostate cancer samples compared with normal tissue (**A**) and of astrocytoma samples compared with normal encephalon (**B**). **C:** A progressive increase in heterogeneity of the percentage of colocalization of CD34 and VIM is associated with increasing grade of cancer, precluding statistical significance. Data are expressed as median (horizontal line in the middle of each box), 75th and 25th percentiles (top and bottom borders of each box, respectively), and 90th and 10th percentiles (whiskers above and below each box, respectively). ***$P < 0.001$ versus normal.

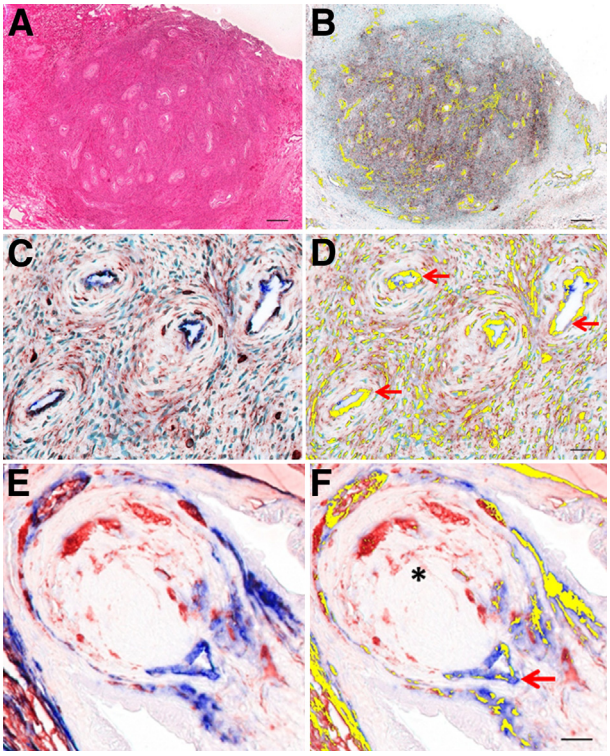

Figure 5 Localization of CD34/VIM dual-positive cells in human BPH tissue and in collagenous micronodules from the TGF-β1 transgenic mouse ventral prostate gland. **A:** H&E-stained section of a stromal nodule. **B:** Deconvoluted image of dual localization (yellow) within stromal nodules. **C:** IHC of CD34 (blue) and VIM (red) within the stromal nodule. **D:** Deconvoluted image of dual localization (yellow) within stromal nodules at higher power shows vasculature (**red arrows**). **E:** Region-enriched VIM-only positive and CD34/VIM$^+$ stromal cells accumulate adjacent to a vessel at the base of a collagenous micronodule in the TGF-β1 transgenic mouse ventral prostate gland. **F:** Deconvoluted image shows CD34 (blue), VIM (red) colocalization pseudo-colored yellow, as well as collagenous micronodule (**asterisk**) and vasculature (**red arrow**). Scale bars: 200 μm (**A** and **B**); 20 μm (**D** and **F**).

proximity to vascular walls with a radial distribution (Figure 5, C and D) similar to the patterns observed in astrocytomas. Of interest, many fibroblast-like cells distributed more distal to vessels were VIM only and lacked CD34 immunoreactivity as observed in Figure 5D. Less regular was the accumulation of CD34/VIM dual-positive fibroblast-like cells adjacent to regions of epithelial hyperplasia. These were restricted to focal patterns in direct association with hyperplastic epithelial acini (data not shown).

CD34/VIM$^+$ Cells in a TGF-β1 Transgenic Mouse Model

To determine whether emergence of CD34/VIM$^+$ fibroblasts were also observed in regions of mouse reactive stroma, we evaluated prostate glands from transgenic mice engineered with TGF-β1 expression targeted to the prostate gland as reported previously.[22] These mice develop collagenous micronodules due to attenuated epithelial lining of secretory acini as a function of age and overexpression of TGF-β1. The collagenous nodules, composed of collagen and reactive stroma, appeared to originate from vessels at the base of epithelial acini and evolved as nodular protrusions into the wall of the acini, effective closing off acini access to the secretory duct. We have reported that this likely occurs as an adaptive process to seal off the acini during breach of the epithelial barrier and disrupted epithelial homeostasis. Although the nodule was composed primarily of collagen extracellular matrix, the cellular elements were found to be composed of both CD34/VIM dual-positive and VIM-only stromal cells (Figure 5, E and F). Similar to observations in human BPH, the core of these nodules contained at least one prominent vessel with CD34-only positive cells and dual-positive CD34/VIM$^+$ cells observed immediately adjacent to vessels (Figure 5F).

CD34/VIM Dual-Positive Cells at the Stromal Invasion Front into Matrigel Plugs and Human Xenograft Tumors

To assess the recruitment of CD34/VIM$^+$ cells during initiation of reactive stroma, subcutaneously inoculated Matrigel plugs and human xenograft tumors constructed with LNCaP prostate cancer cells were evaluated in nude mice. Fibroblast-like cells derived from the mouse host were rapidly recruited to the Matrigel plugs and xenografts in the initial 3 to 5 days after inoculation. Thin layers of Matrigel could be observed in the subcutaneous space at the site of injection in day 4 Matrigel plugs (Figure 6A). Fibroblast-like cells that migrate into the Matrigel plugs were near universally positive for CD34/VIM immunoreactivity (Figure 6, B and C). A similar pattern of recruitment of CD34/VIM$^+$ fibroblast-like cells was observed in the LNCaP xenograft tumors (Figure 6, D–F) with spatial distribution adjacent to clusters of LNCaP cells (Figure 6F).

CD34/VIM Dual-Positive Fibroblasts Originate from Microvasculature Fragments

Microvascular fractions were isolated from mouse adipose tissue as reported previously and evaluated for ability to produce migratory CD34/VIM$^+$ fibroblasts.[27] Adipose tissue from *Flk1-myr::mCherry* transgenic mice were used because of endothelial cell-specific expression of myristoylated mCherry fluorescent protein,[28,29] which was observed in the explants from the vascular fraction (Figure 7, A and B). Microvascular explants cultured on Matrigel-coated coverslips exhibited a distinct tubular shape similar to the one reported in three-dimensional collagen gels (Figure 7C).[27] In contrast to culture on collagen substrates, which produces sprouting and angiogenesis, explants cultured on Matrigel exhibited a reactive stroma phenotype. Cells with distinct fibroblast-like morphology were observed migrating from the vascular tube segments within 12 hours of culture (Figure 7, C and D). The initial wave of cells was dual positive for CD34 and VIM (Figure 7, C and D). At later time points (48 to 72 hours),

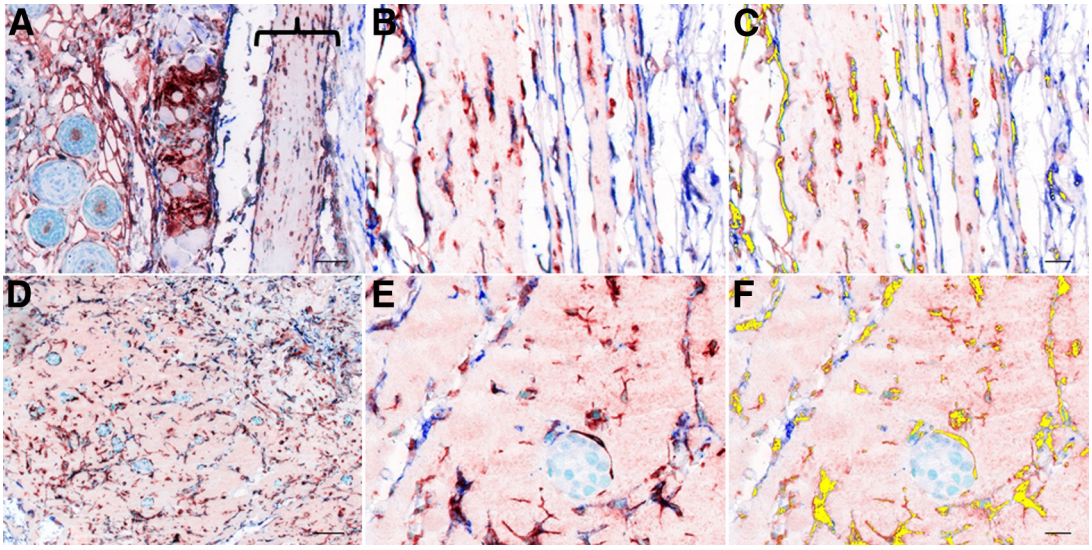

Figure 6 **A**–**C:** Representative micrographs for DRS experiments show invasion of CD34/VIM dual-positive cells into the Matrigel plugs (**A**, **bracket**) as early as 4 days after xenograft implantation, which is maintained until day 10. **D**–**F:** Two-way DRS experiments (Matrigel and LNCaP) show an increased migration of CD34/VIM dual-positive cells into the xenograft. **A:** Dual IHC CD34 (AP, blue) and VIM (HRP, red) of the Matrigel-only xenograft, 10 days after implantation. **B:** Dual IHC CD34 (AP, blue) and VIM (HRP, red) of the Matrigel-only xenograft, 10 days after implantation. Higher magnification of bracketed area from A. **C:** Spectrally deconvoluted image shows colocalization of dual-positive cells pseudo-colored yellow. **D:** Dual IHC for CD34 (AP, blue) and VIM (HRP, red) in the 10-day-old, two-way differential reactive stroma (DRS) xenograft. **E:** Dual IHC for CD34 (AP, blue) and VIM (HRP, red) shows a higher magnification of LNCaP foci within the Matrigel. Higher magnification from **D**. **F:** Spectrally deconvoluted image shows colocalization of dual-positive cells pseudo-colored yellow. Scale bars: 50 μm (**A** and **D**); 20 μm (**C** and **F**).

these cells exhibited attenuated CD34 expression and remained as VIM$^+$ fibroblast-like cells (Figure 7, E and F).

Discussion

We report here that a unique population of CD34/VIM dual-positive reactive stroma fibroblast-like cells is associated with the microenvironment of different human cancers and stromal nodules associated with BPH. In normal tissue, CD34/VIM$^+$ cells were restricted to the microvasculature situated adjacent to the basal lamina of the epithelial layer. Microvascular explants in culture produced CD34/VIM$^+$ cells with a fibroblast phenotype. CD34/VIM$^+$ cells with a fibroblast phenotype were also observed adjacent to the central core vessels in collagenous micronodules in the aged TGF-β1 transgenic mouse prostate gland. Similar CD34/VIM dual-positive fibroblast-like cells were the initial cell type recruited into Matrigel plugs *in vivo* and were the first wave of cells that invade into LNCaP xenograft tumors in nude mice. Cells with an identical phenotype were observed in the reactive stroma and fibrous nodules in human BPH, indicating that recruitment of this reactive stroma cell type is not cancer specific. These cells were associated with thick-walled microvessels commonly observed in the central core of BPH stromal nodules. Consistent with a possible vessel origin, *in vitro* studies indicated that isolated microvasculature generated proliferative and migratory CD34/VIM dual-positive fibroblast-appearing cells.

Data reported here are consistent with previous studies that reported CD34$^+$ stromal-like cells associated with development. During development in the 9- to 15-week-old human fetus, CD34$^+$ cells were observed in vessel structures and were also "distributed diffusely as fibrous tissues," and this was seen in the perimysium and fascia.[30,p919] In addition, that study reported CD34$^+$ fibroblast-like cells observed as fibrous tissue that separated and "bundled" the myocardium. The study concluded that CD34$^+$ stromal cells were critically important in pattern formation of mostly mesenchymal-derived tissues, including skeletal muscle, synovial tissue, and "muscle/tendon-associated tissue."[30,p919] Additional studies suggested that CD34$^+$ mesenchymal tissue was involved in pattern formation in the development of laryngeal and pharyngeal walls.[31] The IHC staining pattern in these studies showed both vessel-like structures, and more diffuse staining described as fibrous tissues was positive for CD34 and VIM.

Appearance of CD34$^+$ cells in the stromal compartment followed by appearance of myofibroblasts has been reported in several adult cancers and tissue disorders, although these cells have never been fully characterized. Appearance and progressive loss of CD34$^+$ cells and gain of smooth muscle alpha actin (ACTA2) positive myofibroblasts have been reported in the reactive stroma in high-grade and invasive mammary cancer,[32] during progression from benign to malignant squamous cell carcinoma,[33] and in progression from squamous intraepithelial lesions to squamous cell carcinoma of the cervix.[34] This same scenario has also been reported adjacent to xanthogranulomatous foci in chronic cholecystitis.[35] It is possible that CD34$^+$ stromal cells set up a patterning template to assist in a more complete stromal

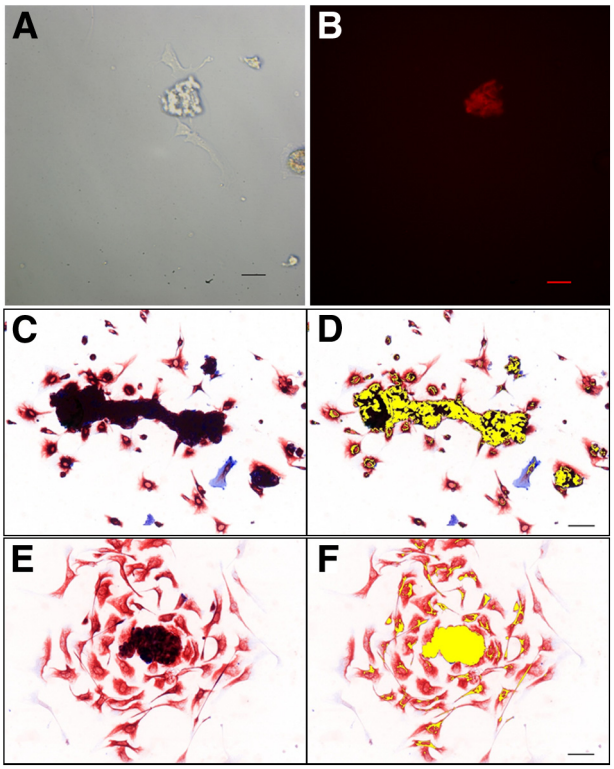

Figure 7 CD34/VIM dual-positive cells expand from microvasculature in culture. Isolated microvasculature explants were identified via positive mCherry expression (**B**) after 12 hours of *in vitro* culture (**A**). **C:** Immunocytochemistry for CD34 (blue) and VIM (red) from 12-hour cultures of murine microvessels. **D:** Deconvolution shows dual-positive cells pseudo-colored yellow. **E:** IHC for CD34 (blue) and VIM (red) from 48-hour cultures of murine microvessels. **F:** Spectral deconvolution shows expansion of dual-positive cells pseudo-colored yellow and VIM-only cells (red only). Scale bars: 50 μm (**A**, **B**, **D**, and **F**).

repair in disrupted adult tissues, analogous to what CD34 stromal cells have been reported to do during patterning in development. It is also possible that $CD34^+$ stromal cells reported here are progenitors of $ACTA2^+$ myofibroblasts. Whether these cell phenotypes originate from different lineages or represent a sequential pattern in a common cell lineage is not understood.

Fibrocytes derived from circulating monocytes can exhibit a fibroblast-like appearance, can express CD34, and have been shown to differentiate to myofibroblasts.[36,37] The proliferative properties and morphology of CD34/VIM cells observed in the microvascular fragment study reported here would suggest these cells are not likely derived from monocytes or fibrocytes. However, we cannot fully rule out this possibility.

Although the precise origin is not yet understood, considerable evidence suggests that the perivascular niche is a site of origin for $CD34/VIM^+$ fibroblast-like stromal cells observed in reactive stroma. Recent studies report that the vessel wall contains three distinct cell types that differentially express CD34. This includes a $CD34^+$/melanoma cell adhesion molecule (MCAM; $CD146)^+$/PECAM1 $(CD31)^+$ endothelial cell, a $CD34^-/MCAM^+$ pericyte, and a $CD34^+/MCAM^-$ "adventitial stromal cell-like cell."[38,p815] The adventitial stromal cell-like cell was able to expand out, become fibroblastoid, and acquired mesenchymal stem cell properties: endoglin$^+$ (ENG; CD105), MCAM$^+$ (CD146), and nerve growth factor receptor$^+$ (NGFR; CD271). As these cells began to expand out via proliferation, expression of CD34 was reduced. In addition, pseudoangiomatous stromal hyperplasia in mammary tissue consists of $CD34^+$ stromal fibroblastoid cells, termed myofibroblasts, which form hyperplastic fibrotic lesions in the pseudo vascular space.[39,40] $CD34^+$ stromal-like cells isolated from the stromal vascular fraction in adipose tissue were capable of forming spheroids, were highly proliferative, and could be induced to differentiate to either adipocytes or $PECAM1^+$ endothelial cells and capillary tubes, suggesting they exhibited stem cell capabilities.[41] Another study found that adherent $CD34^+$ cells isolated from the stromal vascular fraction could be induced to differentiate to different mesenchymal cell types.[42] In addition, $CD34^+$ cells that reside in the periendothelial site in the stromal vascular fraction were shown to express pericyte and mesenchymal markers and functioned to stabilize endothelial networks.[43] Together, these data are consistent with the suggestion that $CD34/VIM^+$ fibroblasts originate from the wall of the local microvasculature. Moreover, these studies suggest that the $CD34^+$ fibroblast-like cells may exhibit mesenchymal stem cell properties, capable of differentiation to different stromal cell types. If true, this would be of obvious value to regaining homeostasis at focal sites of wound repair or tissue remodeling.

It is possible that the microvasculature generates a reactive stroma in response to injury of an adjacent epithelial barrier. Breach of epithelial barrier is the primary lesion in the aged TGF-β1 transgenic mouse prostate gland, where formation of collagenous micronodules that force closure of the secretory acini is promoted.[22] Here too, microvasculature appears to be the most likely source of the emerging CD34/VIM fibroblasts that comprise the rare cells observed in the micronodule, which is composed mostly of extracellular matrix collagen. Because a breach of epithelial barrier function is permissive for microbial intrusion and fluid loss, there is an obvious rationale for a rapid reactive stroma response to restore compartmental homeostasis. Also note that the microvasculature is highly sensitive to tissue disruption. Postcapillary venules are particularly responsive to histamine and other active factors associated with tissue injury and breach of epithelial layers. We propose that the microvasculature is a potent regulator of the reactive stroma response in tissue disruption or loss of homeostasis as occurs in cancer and benign proliferative disorders. In addition, we propose that activation and recruitment of $CD34/VIM^+$ fibroblast-like cells from the microvasculature occurs as the initial wave of first responders in disrupted tissue homeostasis. Understanding the origin, recruitment, and biology of the $CD34/VIM^+$ cells in tumor tissue and in repair tissue is important in the development of novel

therapeutic approaches designed to target the tumor microenvironment, benign stromal disorders such as BPH, or abnormal tissue repair disorders.

Acknowledgments

We thank Deedee Killien (Baylor College of Medicine) in the IHC staining of the human tissue arrays, Drs. Mary Dickinson and Ross Poche (Baylor College of Medicine) for kindly providing the *Flk1-myr::mCherry*$^{+/tg}$ mice, and the support of the Genetically Engineered Mouse Shared Resource and Human Tissue Acquisition and Pathology Shared Resource at Baylor College of Medicine.

Supplemental Data

Supplemental material for this article can be found at *http://dx.doi.org/10.1016/j.ajpath.2014.02.021*.

References

1. Tuxhorn JA, Ayala GE, Rowley DR: Reactive stroma in prostate cancer progression. J Urol 2001, 166:2472−2483
2. Tuxhorn JA, Ayala GE, Smith MJ, Smith VC, Dang TD, Rowley DR: Reactive stroma in human prostate cancer: induction of myofibroblast phenotype and extracellular matrix remodeling. Clin Cancer Res 2002, 8:2912−2923
3. Desmouliere A, Geinoz A, Gabbiani F, Gabbiani G: Transforming growth factor-beta 1 induces alpha-smooth muscle actin expression in granulation tissue myofibroblasts and in quiescent and growing cultured fibroblasts. J Cell Biol 1993, 122:103−111
4. Desmouliere A, Chaponnier C, Gabbiani G: Tissue repair, contraction, and the myofibroblast. Wound Repair Regen 2005, 13:7−12
5. Dvorak HF: Tumors: wounds that do not heal. Similarities between tumor stroma generation and wound healing. N Engl J Med 1986, 315: 1650−1659
6. Orimo A, Gupta PB, Sgroi DC, Arenzana-Seisdedos F, Delaunay T, Naeem R, Carey VJ, Richardson AL, Weinberg RA: Stromal fibroblasts present in invasive human breast carcinomas promote tumor growth and angiogenesis through elevated SDF-1/CXCL12 secretion. Cell 2005, 121:335−348
7. Liao D, Luo Y, Markowitz D, Xiang R, Reisfeld RA: Cancer associated fibroblasts promote tumor growth and metastasis by modulating the tumor immune microenvironment in a 4T1 murine breast cancer model. PLoS One 2009, 4:e7965
8. Olumi AF, Grossfeld GD, Hayward SW, Carroll PR, Tlsty TD, Cunha GR: Carcinoma-associated fibroblasts direct tumor progression of initiated human prostatic epithelium. Cancer Res 1999, 59: 5002−5011
9. Verona EV, Elkahloun AG, Yang J, Bandyopadhyay A, Yeh IT, Sun LZ: Transforming growth factor-beta signaling in prostate stromal cells supports prostate carcinoma growth by up-regulating stromal genes related to tissue remodeling. Cancer Res 2007, 67:5737−5746
10. Ohuchida K, Mizumoto K, Murakami M, Qian LW, Sato N, Nagai E, Matsumoto K, Nakamura T, Tanaka M: Radiation to stromal fibroblasts increases invasiveness of pancreatic cancer cells through tumor-stromal interactions. Cancer Res 2004, 64:3215−3222
11. Lijnen P, Petrov V, Rumilla K, Fagard R: Transforming growth factor-beta 1 promotes contraction of collagen gel by cardiac fibroblasts through their differentiation into myofibroblasts. Methods Find Exp Clin Pharmacol 2003, 25:79−86
12. Kirk TZ, Mark ME, Chua CC, Chua BH, Mayes MD: Myofibroblasts from scleroderma skin synthesize elevated levels of collagen and tissue inhibitor of metalloproteinase (TIMP-1) with two forms of TIMP-1. J Biol Chem 1995, 270:3423−3428
13. Grotendorst GR, Duncan MR: Individual domains of connective tissue growth factor regulate fibroblast proliferation and myofibroblast differentiation. FASEB J 2005, 19:729−738
14. De Wever O, Nguyen QD, Van Hoorde L, Bracke M, Bruyneel E, Gespach C, Mareel M: Tenascin-C and SF/HGF produced by myofibroblasts in vitro provide convergent pro-invasive signals to human colon cancer cells through RhoA and Rac. FASEB J 2004, 18:1016−1018
15. Stuelten CH, DaCosta Byfield S, Arany PR, Karpova TS, Stetler-Stevenson WG, Roberts AB: Breast cancer cells induce stromal fibroblasts to express MMP-9 via secretion of TNF-alpha and TGF-beta. J Cell Sci 2005, 118:2143−2153
16. Taniwaki K, Fukamachi H, Komori K, Ohtake Y, Nonaka T, Sakamoto T, Shiomi T, Okada Y, Itoh T, Itohara S, Seiki M, Yana I: Stroma-derived matrix metalloproteinase (MMP)-2 promotes membrane type 1-MMP-dependent tumor growth in mice. Cancer Res 2007, 67:4311−4319
17. Dandachi N, Hauser-Kronberger C, More E, Wiesener B, Hacker GW, Dietze O, Wirl G: Co-expression of tenascin-C and vimentin in human breast cancer cells indicates phenotypic transdifferentiation during tumour progression: correlation with histopathological parameters, hormone receptors, and oncoproteins. J Pathol 2001, 193:181−189
18. Huang W, Chiquet-Ehrismann R, Moyano JV, Garcia-Pardo A, Orend G: Interference of tenascin-C with syndecan-4 binding to fibronectin blocks cell adhesion and stimulates tumor cell proliferation. Cancer Res 2001, 61:8586−8594
19. Adams M, Jones JL, Walker RA, Pringle JH, Bell SC: Changes in tenascin-C isoform expression in invasive and preinvasive breast disease. Cancer Res 2002, 62:3289−3297
20. Adamsky K, Schilling J, Garwood J, Faissner A, Peles E: Glial tumor cell adhesion is mediated by binding of the FNIII domain of receptor protein tyrosine phosphatase beta (RPTPbeta) to tenascin C. Oncogene 2001, 20:609−618
21. Schauer IG, Ressler SJ, Tuxhorn JA, Dang TD, Rowley DR: Elevated epithelial expression of interleukin-8 correlates with myofibroblast reactive stroma in benign prostatic hyperplasia. Urology 2008, 72: 205−213
22. Barron DA, Strand DW, Ressler SJ, Dang TD, Hayward SW, Yang F, Ayala GE, Ittmann M, Rowley DR: TGF-beta1 induces an age-dependent inflammation of nerve ganglia and fibroplasia in the prostate gland stroma of a novel transgenic mouse. PLoS One 2010, 5:e13751
23. Tuxhorn JA, McAlhany SJ, Dang TD, Ayala GE, Rowley DR: Stromal cells promote angiogenesis and growth of human prostate tumors in a differential reactive stroma (DRS) xenograft model. Cancer Res 2002, 62:3298−3307
24. McAlhany SJ, Ressler SJ, Larsen M, Tuxhorn JA, Yang F, Dang TD, Rowley DR: Promotion of angiogenesis by ps20 in the differential reactive stroma prostate cancer xenograft model. Cancer Res 2003, 63: 5859−5865
25. Yang F, Strand DW, Rowley DR: Fibroblast growth factor-2 mediates transforming growth factor-beta action in prostate cancer reactive stroma. Oncogene 2008, 27:450−459
26. Yang F, Tuxhorn JA, Ressler SJ, McAlhany SJ, Dang TD, Rowley DR: Stromal expression of connective tissue growth factor promotes angiogenesis and prostate cancer tumorigenesis. Cancer Res 2005, 65:8887−8895
27. Reed MJ, Damodarasamy M, Vernon RB: Angiogenesis In Vitro utilizing Murine Vascular Explants in Miniaturized 3-Dimensional Collagen Gels. Open Circ Vasc J 2011, 4:12−17
28. Larina IV, Shen W, Kelly OG, Hadjantonakis AK, Baron MH, Dickinson ME: A membrane associated mCherry fluorescent reporter line for studying vascular remodeling and cardiac function during murine embryonic development. Anat Rec (Hoboken) 2009, 292: 333−341

29. Poche RA, Larina IV, Scott ML, Saik JE, West JL, Dickinson ME: The Flk1-myr::mCherry mouse as a useful reporter to characterize multiple aspects of ocular blood vessel development and disease. Dev Dyn 2009, 238:2318–2326
30. Abe S, Suzuki M, Cho KH, Murakami G, Cho BH, Ide Y: CD34-positive developing vessels and other structures in human fetuses: an immunohistochemical study. Surg Radiol Anat 2011, 33:919–927
31. Katori Y, Kiyokawa H, Kawase T, Murakami G, Cho BH: CD34-positive primitive vessels and other structures in human fetuses: an immunohistochemical study. Acta Otolaryngol 2011, 131:1086–1090
32. Catteau X, Simon P, Vanhaeverbeek M, Noel JC: Variable stromal periductular expression of CD34 and smooth muscle actin (SMA) in intraductal carcinoma of the breast. PLoS One 2013, 8:e57773
33. Kacar A, Arikok AT, Kokenek Unal TD, Onder E, Hucumenoglu S, Alper M: Stromal expression of CD34, alpha-smooth muscle actin and CD26/DPPIV in squamous cell carcinoma of the skin: a comparative immunohistochemical study. Pathol Oncol Res 2012, 18:25–31
34. Li Q, Huang W, Zhou X: Expression of CD34, alpha-smooth muscle actin and transforming growth factor-beta1 in squamous intraepithelial lesions and squamous cell carcinoma of the cervix. J Int Med Res 2009, 37:446–454
35. Kuroda N, Guo L, Miyazaki E, Hamauzu T, Toi M, Hiroi M, Enzan H: The appearance of myofibroblasts and the disappearance of CD34-positive stromal cells in the area adjacent to xanthogranulomatous foci of chronic cholecystitis. Histol Histopathol 2005, 20:127–133
36. Pilling D, Vakil V, Gomer RH: Improved serum-free culture conditions for the differentiation of human and murine fibrocytes. J Immunol Methods 2009, 351:62–70
37. Quan TE, Cowper S, Wu SP, Bockenstedt LK, Bucala R: Circulating fibrocytes: collagen-secreting cells of the peripheral blood. Int J Biochem Cell Biol 2004, 36:598–606
38. Braun J, Kurtz A, Barutcu N, Bodo J, Thiel A, Dong J: Concerted regulation of CD34 and CD105 accompanies mesenchymal stromal cell derivation from human adventitial stromal cell. Stem Cells Dev 2013, 22:815–827
39. Donk WA, Oostenbroek RJ, Storm RK, Westenend PJ, Plaisier PW: Pseudoangiomatous Stromal Hyperplasia: Diagnosis, Treatment and Follow-Up; Description of a Case-Series. Open Breast Cancer Journal 2011, 3:18–23
40. Virk RK, Khan A: Pseudoangiomatous stromal hyperplasia: an overview. Arch Pathol Lab Med 2010, 134:1070–1074
41. De Francesco F, Tirino V, Desiderio V, Ferraro G, D'Andrea F, Giuliano M, Libondi G, Pirozzi G, De Rosa A, Papaccio G: Human CD34/CD90 ASCs are capable of growing as sphere clusters, producing high levels of VEGF and forming capillaries. PLoS One 2009, 4:e6537
42. Eto H, Ishimine H, Kinoshita K, Watanabe-Susaki K, Kato H, Doi K, Kuno S, Kurisaki A, Yoshimura K: Characterization of human adipose tissue-resident hematopoietic cell populations reveals a novel macrophage subpopulation with CD34 expression and mesenchymal multipotency. Stem Cells Dev 2013, 22:985–997
43. Traktuev DO, Merfeld-Clauss S, Li J, Kolonin M, Arap W, Pasqualini R, Johnstone BH, March KL: A population of multipotent CD34-positive adipose stromal cells share pericyte and mesenchymal surface markers, reside in a periendothelial location, and stabilize endothelial networks. Circ Res 2008, 102:77–85